

Facilitating target search in polymer networks: Effects of target size and mixed one-dimensional and three-dimensional diffusion

Xiao Xu ¹, Won Kyu Kim ^{2,*} and Joachim Dzubiella ^{3,4,†}

¹*School of Chemical Engineering, Nanjing University of Science and Technology, 200 Xiao Ling Wei, Nanjing 210094, People's Republic of China*

²*Korea Institute for Advanced Study, 85 Hoegiro, Seoul 02455, Republic of Korea*

³*Research Group for Simulations of Energy Materials, Helmholtz-Zentrum Berlin für Materialien und Energie, Hahn-Meitner-Platz 1, D-14109 Berlin, Germany*

⁴*Physikalisches Institut, Albert-Ludwigs-Universität Freiburg, Hermann-Herder Strasse 3, D-79104 Freiburg, Germany*

 (Received 4 August 2020; revised 10 December 2020; accepted 13 February 2021; published 11 March 2021)

We theoretically investigate the problem of diffusive target search and mean first passage times (MFPTs) of a tracer in a three-dimensional (3D) polymer network with a particular focus on the effects of combined one-dimensional (1D) diffusion along the polymer chains and 3D diffusion within the network. For this, we employ computer simulations as well as limiting theories of a single diffusive tracer searching for a spherical target fixed at a cross-link of a homogeneous 3D cubic lattice network. The free parameters are the target size, the ratio of the 1D and 3D friction constants, and the transition probabilities between bound and unbound states. For a very strongly bound tracer on the chains, the expected predominant set of 1D lattice diffusion (LD) is found. The MFPT in the LD process significantly depends on the target size, yielding two distinct scaling behaviors for target sizes smaller and larger than the network mesh size, respectively. In the limit of a pointlike target, the LD search becomes a random walk process on the lattice, which recovers the analytical solution for the MFPT previously reported by S. Condamin, O. Bénichou, and M. Moreau [*Phys. Rev. Lett.* **95**, 260601 (2005)]. For the very weakly bound tracer, the expected 3D free diffusion (FD) dominates, extrapolating to the well-known Smoluchowski limit. A critical target size is found above which the MFPT in the FD process is faster than in the LD process. For intermediate binding, i.e., a combination of LD and FD processes, the target search time can be minimized for an optimal range of target sizes and partitions between FD and LD, for which the MFPTs are substantially faster when compared to the limiting FD or LD processes. Our study may provide a theoretical basis to better understand and predict search and reaction processes in complex structured materials, thereby contributing to practical applications such as designing nanoreactors where catalytic targets are immobilized in polymer networks.

DOI: [10.1103/PhysRevE.103.032502](https://doi.org/10.1103/PhysRevE.103.032502)

I. INTRODUCTION

Target search in complex topologies is a wide and important field of study [1–9]. For example, the target search by biomolecules in cells is rapid and specific, being the basis of many biological processes [10]. Most prominently, DNA-binding proteins locate targets on DNA in a sequence-specific manner, and transfer genetic information [1]. A specific target search is similarly observed in coordinated chemical reactions [2,3]. The target search problem is also found on the macroscopic level, such as animals chasing food [4–6] and castaway rescue operations [7]. Such a multiscale nature of target search processes makes the problem not only challenging but also demands a better theoretical understanding.

Various target search strategies have been revealed and confirmed theoretically to possess remarkable promptitude and fidelity [4,8]. Fast localization rates generally require

intermittent search strategies, which employ multiple phases within the search process [9]. The most well-known example is the protein search for small pieces of specific DNA sequences, which is modeled by a combination of three-dimensional (3D) diffusion in the bulk solution and one-dimensional (1D) “sliding” along the DNA chain [11,12], corresponding to the fast kinetics for protein translocation and probing different DNA fragments, and the slower but locally more efficient phase to detect the small target on the 1D chain, respectively. The resultant target search rate substantially exceeds the 3D limit [13], given by the well-known Debye-Smoluchowski rate theory [14].

Many theoretical and numerical efforts have been made to build up a qualitative and quantitative understanding of intermittent search strategies [4,15,16]. The most widely known and utilized example is the Berg-Winter-Hippel (BWH) model [17] consisting of multiple 1D and 3D diffusion processes. In the protein-DNA case mentioned above, according to this model, the target search time can be minimized by a delicately weighted partition of the 1D and 3D diffusion time [1,17]. If the 3D diffusion time is above that partition, the search time

*wonkyukim@kias.re.kr

†joachim.dzubiella@physik.uni-freiburg.de

is spent mostly in the bulk via 3D diffusion. Otherwise, the protein diffuses mostly (typically slowly) on the DNA chain, which ends up with a very local and repeated sampling of the DNA sites [18]; thus both cases alone impede an efficient search. To capture the optimal partition of the 1D and 3D diffusion, one requires a specific knowledge of the target size [19,20], chain configuration [9,21,22], protein flexibility [23], sequence dependence [23,24], and hydrodynamic effects [25].

Understanding the target search problem in such confined geometries is also important for the development of fast chemical reactions using advanced polymeric materials. A practical example related to reaction-diffusion processes operating in different geometries is the case of responsive nanoreactors, possessing great potential in nanocatalysis [26–35]. One of the main characteristics of these systems is the presence of a stimuli-responsive polymeric network (nano- or micro-hydrogel), forming a permeable shell around catalytic targets, e.g., nanoparticles or enzymes, where reactants can penetrate through the shell from a bulk space. Other applications can be seen in the metal-organic frameworks (MOFs) and porous coordination polymers [29,36]. The catalytic activity thus can be tuned in response to external stimuli such as temperature and solvent quality [28,29,33]. The simplest theoretical description would be the diffusion-controlled picture [37–39], e.g., where the intrinsic catalytic reaction (on the catalyst surface) is instantaneous; therefore the total reaction rate is governed only by the diffusive search time of the reactant to the target nanoparticle in the polymer matrix. Inspired by the protein-DNA target search problem, it would be natural to ask if the polymer matrix can be engineered such that the catalytic activity of the nanoreactor is enhanced by intermittent 1D and 3D excursions of the penetrating reactants.

Regarding the reactant in the polymeric matrix as a point-like diffusive tracer in a 3D network, the related target search process can be considered for a start as a collection of discrete and random jumps between the network cross-links. The mean first passage time (MFPT) for such a random walker moving between two arbitrary sites was systematically studied in random networks [40]. These studies were extended by introducing extra target sites on the lattice [41–43], and proposed accurate estimations of the MFPT between the sites, as an exact solution of the target search time of discrete random walks. An extension of this method has been developed to describing continuous Brownian motion [41], and is thus promising to bring a quantitative understanding of the search mechanism on lattice sites. However, a theoretical approach for the target search problem in terms of stochastic processes inside polymer networks is still lacking. In addition, to the best of our knowledge, there is no study assessing the combined 1D-3D search in the polymer chain lattice, despite that the full 1D and 3D search behaviors have been well understood individually. More importantly, effects of the target size on the target search time still remain unknown, particularly in polymer networks, which we tackle to resolve in this work.

To better understand the target search process in polymer networks, in this paper we consider a simple model, which approximates a real polymer network by a simple cubic lattice, comprising stiff and stretched chains [44,45]. Using the model, we investigate the target search problem by performing stochastic numerical simulations and presenting limiting

analytical theories for the target search time. As shown in Fig. 1, we focus on regular polymer networks (of idealized stiff polymer chains) on the cubic lattice of mesh size l_x that we use as a unit length, where a spherical target of adjustable radius l_t is located at one of the lattice cross-links in the center of the simulation box. Given a tracer performing lattice diffusion (LD), the analytical expression of the target search time is derived as a function of the target size l_t . The intermittent search as a combination of the LD and free diffusion (FD) is then investigated by the simulations. We find that the search time efficiency can be enhanced in the intermittent search, significantly depending on the target size, and is markedly faster in comparison with the limiting cases with LD or FD only.

II. MODEL AND METHODS

A. Model and length scales

As illustrated in Fig. 1, the simulation model consists of a regular polymer network on a simple cubic lattice, consisting of stiff polymers of monodisperse length. The simulation box has the length $2L$ and is subject to the periodic boundary condition in 3D. The cubic lattice has the mesh size l_x , which is treated as the unit length, and the number of unit cells is $N_{\text{cell}} = (2L)^3$. The tracer diffuses in the polymer network until it contacts the target located at the cross-link position r_S of the simulation box center. The target is considered as a hard sphere of radius l_t , where the search process terminates when the tracer reaches the target surface. The box size $L = 10$ is fixed, and the target size l_t is an adjustable parameter.

The tracer may stay bound on the polymers (in 1D) or unbound (in 3D), corresponding to the target search as a combination of lattice diffusion (LD) and free diffusion (FD). The polymer thickness l_e determines the adsorption range and thus the type of the search process, LD or FD. Namely, the tracer is deemed bound (and thus under LD) when it is within the lateral distance l_e from any polymer axes, whereas the tracer in the remaining areas is considered as being in the unbound phase and performing FD [see Figs. 1(b) and 1(d)]. In the simulation, we set $l_e = 0.05$ such that the polymer adsorption thickness is sufficiently small to ensure the LD. The bound-unbound switching between the LD and the FD, as similarly found between DNA and proteins [46,47], is considered as a simple two-state Markovian chain. We thus consider a transition probability p_{on} of the tracer for moving from the unbound state toward the bound state on the polymer chain of diameter $2l_e$, as illustrated in Figs. 1(d) and 1(e). Therefore, a transition probability for remaining in the unbound state is $p_{\text{UU}} = 1 - p_{\text{on}}$. We also consider a transition probability p_{off} for moving from the bound to unbound state, thereby having a transition probability for staying in the bound state as $p_{\text{BB}} = 1 - p_{\text{off}}$. In this sense, the two transitions (bound to unbound and vice versa) are completely independent, thus Markovian. In addition, our model ensures the detailed balance [48], which will be discussed later in more detail. We vary the desorption transition probability p_{off} from 0 to 1, while the adsorption transition probability p_{on} is fixed to unity, as similarly used in protein-DNA models [46,47]. Namely, the diffusion switches to the LD as soon as the free tracer in the bulk phase enters the bound phase with the probability $p_{\text{on}} = 1$. Inversely but independently, the bound tracer may

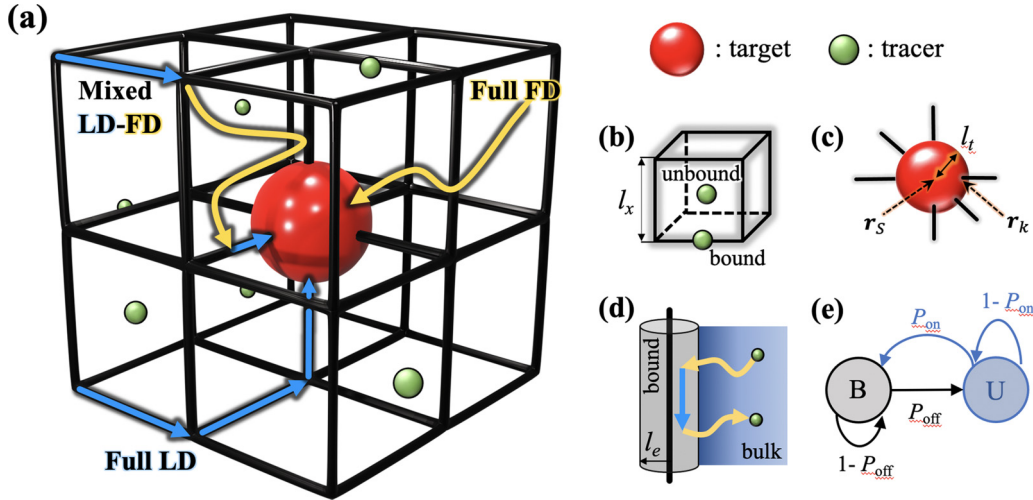


FIG. 1. Left: Illustration of the target search model. Right: Explanatory legend. (a) The cubic lattice network (displayed here are only the 8 cubic cells connecting with the target) with the mesh size $l_x = 1$. Three representative trajectories of the multiple independent tracers (green sphere) approaching the target (red sphere) are illustrated for the full lattice diffusion (LD), full free diffusion (FD), and combined LD-FD search, respectively, colored in blue and yellow. (b) A unit cell of the chain lattice of the mesh size $l_x = 1$, illustrating the unbound and bound states. (c) The target has the radius l_t and is fixed at the lattice cross-link located at the simulation box center. During the LD search, the tracer reaches the target at the target-chain intersecting points. The target-chain intersection points and the target center position ($l_t < 1$ in this example) are denoted by r_k and r_s , respectively. (d) The tracer can bind on the chains in the coaxial cylindrical region of the radius l_e . The bound area is highlighted in gray, while the bulk phase is sketched in blue. The trajectory switching the tracer from the FD search to the LD search and finally back to the FD search is depicted. (e) Illustration of the underlying two-state Markov process of the search process. The gray and blue circles denote the bound and unbound states of the tracer, respectively.

be released toward the bulk space with the probability p_{off} that we vary as a parameter. Note that the adsorption and desorption events are considered only if the tracer is within the polymer adsorption range l_e . The desorption probability p_{off} has two important search limits: the pure LD search as $p_{\text{off}} \rightarrow 0$ and the FD search limit (not exactly full FD search, but FD is dominant given the thin polymer chains) as $p_{\text{off}} \rightarrow 1$.

B. Simulations and methods

The tracer diffusion dynamics illustrated in Fig. 1 is simulated by overdamped Langevin dynamics for the bound tracer position \mathbf{X}_{LD} in the LD, or the unbound tracer position \mathbf{X}_{FD} in the FD, via

$$\frac{d\mathbf{X}_{\text{LD}}(t)}{dt} = \mathbf{R}_{\text{LD}}(t), \quad (1a)$$

$$\frac{d\mathbf{X}_{\text{FD}}(t)}{dt} = \mathbf{R}_{\text{FD}}(t), \quad (1b)$$

where the choice of bound and unbound positions depends on the lateral distance of the tracer from the closest polymer axis, r_c , and the transition probabilities p_{on} and p_{off} . Equation (1a) describes the LD on the polymers ($0 < r_c \leq l_e$), which is essentially a collection of 1D diffusion on the polymers in 3D space, while Eq. (1b) is for the FD in the bulk. At every time step, the lateral distance r_c is calculated. When the tracer previously in the bulk ($r_c > l_e$) binds to the polymer ($r_c \leq l_e$), the dynamics is switched to the LD with the probability p_{on} and follows Eq. (1a). During the LD search along the polymers, the tracer can move to another neighboring polymer by passing through cross-links in a random fashion,

until it is unbound with the probability p_{off} , which switches the dynamics from the LD to the FD that follows Eq. (1b). Thus, in fact, the latter is used always when $r_c > l_e$, or if $r_c \leq l_e$ and after being transforming from LD to FD with probability p_{off} . The above computational scheme is in the spirit of the kinetic Monte Carlo simulation, which serves as a simple and robust approach for studying systems evolving through random walks and state transformations [49–53]. The random forces $\mathbf{R}_{\text{LD}}(t)$ and $\mathbf{R}_{\text{FD}}(t)$ in Eq. (1) have zero means and correlations satisfying the fluctuation-dissipation theorem [54],

$$\begin{aligned} \langle R_{\text{LD}}^i(t) R_{\text{LD}}^j(t') \rangle &= 2k_{\text{B}}T \delta(t - t') \delta_{ij} / \gamma_1, \quad i = x, y, z, \\ \langle R_{\text{FD}}^i(t) R_{\text{FD}}^j(t') \rangle &= 2k_{\text{B}}T \delta(t - t') \delta_{ij} / \gamma_3, \quad i = x, y, z, \end{aligned} \quad (2)$$

where $k_{\text{B}}T \equiv 1/\beta$ is the thermal energy, and γ_1 and γ_3 are the respective friction coefficients for the LD and the FD. Recent studies revealed that the 1D diffusion of a protein (such as the transcription factor [55]) on a DNA chain appears to be much slower than in the bulk solutions [1,56,57]. Therefore, defining the friction ratio as $q \equiv \gamma_3/\gamma_1$, we focus on the range $0 < q \leq 1$.

The tracer is initially located randomly at one of six centers of the box boundary surfaces. The characteristic timescale is set as $\tau_x = \beta\gamma_1/2$, corresponding to the mean number of the time steps to diffuse over two adjacent cross-links via the LD search, namely, the average time for the tracer diffusing along a polymer between two adjacent cross-links. For our case, $\tau_x = 400$ in units of the simulation time step is set throughout the study. The simulations generate many target search processes with numerous mixture of the FD and LD, by tuning the desorption transition probability p_{off} , the friction

ratio q , and the target size l_t . For each set of parameters, at least 10^3 independent runs are carried out for better statistics.

The central quantity of this numerical study is the mean first passage time τ for the tracer to find the target particle, starting from the initial position. The total target search process minimizing the time τ , tuned by the above parameters, is of particular interest.

C. Analytical results

Before showing our numerical results, we introduce corresponding analytical results to some limiting cases that we consider. For simplicity, now we use the subscript index “1” for the LD and “3” for the FD.

1. Full FD process, $p_{\text{on}} = 0$, $p_{\text{off}} = 1$

In this simplest regime, our model reduces to the target search problem in the bulk solution. An approximate solution of the tracer MFPT with the periodic boundary condition yields [42]

$$\tau_3 = \frac{V\beta\gamma_3}{4\pi} \left(\frac{1}{l_t} - \frac{1}{L} \right), \quad (3)$$

where $V = (2L)^3$ is the box volume, and L corresponds to the initial tracer-target distance. An exact but lengthy expression of τ_3 can be found in Ref. [58], yet we only adopt Eq. (3) here to keep the discussions concise. Given the timescale τ_x , Eq. (3) is rewritten as

$$\frac{\tau_3}{\tau_x} = \frac{qV}{2\pi} \left(\frac{1}{l_t} - \frac{1}{L} \right). \quad (4)$$

For an infinitely large system with $L \rightarrow \infty$, Eq. (4) reduces to the Smoluchowski search time [14]

$$\frac{\tau_{\text{Smo}}}{\tau_x} = \frac{qV}{2\pi l_t}. \quad (5)$$

2. Full LD process with a pointlike target,

$$p_{\text{on}} = 1, p_{\text{off}} = 0, l_t \rightarrow 0$$

The condition $p_{\text{on}} = 1$ and $p_{\text{off}} = 0$ gives rise to a persistent LD mode, diffusing over $N = (2L + 1)^3$ lattice cross-links with one of them being the pointlike target. The corresponding MFPT $\tau_1|_{l_t=0}$ can be derived from a random walk process from an initial position at \mathbf{r}_T to the target position at \mathbf{r}_S (see also in Fig. 1), which is a series of random jumps between adjacent lattice cross-links. In this case, the MFPT solution $\tau_1|_{l_t=0}$ is given by Condamin [41,42] as

$$\tau_1|_{l_t=0} = \tau_x N [H(\mathbf{r}_S|\mathbf{r}_S) - H(\mathbf{r}_S|\mathbf{r}_T)], \quad (6)$$

where $H(\mathbf{r}_i|\mathbf{r}_j)$ is the pseudo Green’s function (see Appendix) between cross-link positions \mathbf{r}_i and \mathbf{r}_j . It should be mentioned that the theory originally considered a lattice with reflecting boundary conditions, which also applies to our simulation given that the target is placed at the lattice point right in the center of the periodic cubic box. In case of \mathbf{r}_T sufficiently far from \mathbf{r}_S , $\tau_1|_{l_t=0}$ approaches its upper limit $\tau_x N H(\mathbf{r}_S|\mathbf{r}_S)$, which is found finite for the cubic lattice [59]. This brings out a stark contrast with Eq. (4), where τ_3 for the full FD search is proportional to l_t^{-1} and thus diverges in the limit of the pointlike target size $l_t \rightarrow 0$.

3. Full LD process, $p_{\text{on}} = 1$, $p_{\text{off}} = 0$ with $l_t \gg 1$

Now we extend the previous case where the spherical target on a cross-link has a finite size. In this case, as opposed to the FD search, the LD search process involves a finite set of multiple intersecting points on the target surface, which coincide with the lattice chains. To understand such a complex situation, we consider a limiting case: For a target of radius sufficiently larger than the lattice mesh size, $l_t \gg 1$, the intersecting surface points becomes continuous, making the dynamic behavior of the LD search converging to the FD search. Recalling that the LD search performs a combination of 1D diffusion and is randomly redirected at each cross-linker, in the long time limit, the diffusion time along an arbitrary direction i tends to be $t_i = t/3$ on average. Consequently, the limiting LD diffusivity $D_{\text{LD}} = k_B T / (3\gamma_1)$ yields the target search time

$$\tau_1|_{l_t \gg 1} = \tau_x \frac{3N}{2\pi l_t}, \quad (7)$$

by rewriting Eq. (5) in this limiting case. Therefore, we find from this analysis in the large-target approximation how a full LD search incorporates the dependency on the target size.

4. Full LD process, $p_{\text{on}} = 1$, $p_{\text{off}} = 0$ with $0 \leq l_t \leq 1$

To take the target size in a continuous range $0 \leq l_t \leq 1$ into account, we consider $j = S_{\text{sec}}(r) \nabla \rho(r) / (\beta\gamma_1)$ as the net density current of the tracer at the radial distance r away from the target center. Here, $S_{\text{sec}}(r)$ denotes the total distance-resolved cross-sectional area that the tracer can pass through, and $\rho(r)$ refers to the tracer concentration distribution function. Note that in the steady state, in general the current j is independent of the radial distance r .

For the LD tracer and the target with size $l_t \leq 1$, the cross-section area for the tracer is indeed a constant, say S_0 . To ensure a constant j , the concentration function should be a linear function of r , expressed as

$$\rho(r) = \rho_1(l_t) \left(\frac{r}{1-l_t} - \frac{l_t}{1-l_t} \right), \quad l_t \leq r \leq 1. \quad (8)$$

The proposed $\rho(r)$ complies with two boundary conditions: $\rho(r = l_t) = 0$ at the target surface, and $\rho(r = 1) = \rho_1$, denoting the tracer density at the distance $r = 1$. ρ_1 is affected by the target size, thus a function of l_t . The MFPT is then calculated via $\tau_1|_{0 \leq l_t \leq 1} = 1/j$ as

$$\tau_1|_{0 \leq l_t \leq 1} = \tau_x \frac{2(1-l_t)}{S_0 \rho_1(l_t)}, \quad 0 \leq l_t \leq 1. \quad (9)$$

For the limiting case of $l_t = 0$, Eq. (9) converges to $2\tau_x / [S_0 \rho_1(0)]$, which recovers the search time $\tau_1|_{l_t=0}$ for an infinitely small target indicated by Eq. (6), following

$$\tau_1|_{l_t \rightarrow 0} = \tau_1|_{l_t=0} \times (1-l_t). \quad (10)$$

Thus, a linear dependence of the search time with the target radius l_t is found in the limit of $l_t \rightarrow 0$. We note here that in the limit of the small target, the target is essentially represented by a set of six points, which converges to a single point in the limit of $l_t = 0$, accompanied by a saturated target search time $\tau_1|_{l_t=0}$.

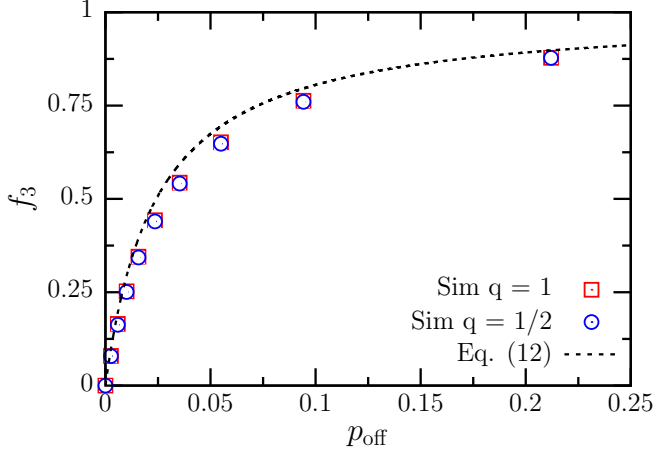


FIG. 2. The time fraction f_3 for the tracer for FD as a function of the desorption probability p_{off} for the friction ratio parameter values of $q = 1$ and $q = 1/2$. The open symbols and the dashed line depict the results from the computer simulation and the theory given in Eq. (12), respectively. In the simulation, we use the target size $l_t = 0.02$ and the absorption probability $p_{\text{on}} = 1$.

5. Mixed LD and FD, $p_{\text{on}} = 1$, $0 < p_{\text{off}} < 1$

Now we focus on the case where the tracer can carry out the search in the combination of the LD and the FD, i.e., $0 < p_{\text{off}} < 1$. This mimics the search process in the presence of an effective adsorption energy $\beta\epsilon_b$ between the tracer and the polymer. The partition function of the tracer in the unit cubic cell [see Fig. 1(b)] is then written as [48]

$$\begin{aligned} Z_t &= \int_{\text{cell/polymer}} dV + \int_{\text{polymer}} e^{-\beta\epsilon_b} dV \\ &= V_3 + \exp(-\beta\epsilon_b)V_1. \end{aligned} \quad (11)$$

Here, $\exp(-\beta\epsilon_b) = p_{\text{on}}/p_{\text{off}}$ is the Boltzmann factor. $V_1 = 3\pi l_e^2$ comprises three cylindrical volumes with radius l_e per

cubic cell, while the rest space of volume $V_3 = 1 - 3\pi l_e^2$ is left for the FD tracer. The time fraction of the tracer executing the FD or the LD search should be proportional to the effective volume of the respective regime, which leads to the expression for the time fraction of the FD as

$$f_3 = \frac{V_3}{V_3 + V_1 p_{\text{on}}/p_{\text{off}}}. \quad (12)$$

Here, the unit cell is composed of two subregions with the effective volume V_3 and $V_1 p_{\text{on}}/p_{\text{off}}$, respectively.

Note that the above theory aims at establishing the equilibrium distribution of the tracer in the absence of the target. Thus, a meaningful comparison between the theory and the simulation should be made only for small targets. In Fig. 2, we present the simulation result of f_3 with the target size $l_t = 0.02$ as a function of the desorption probability p_{off} . As expected, f_3 depicting the time fraction of the tracer in the unbound state is found almost independent of the friction ratio q . Moreover, a good agreement between the simulation result and the theory is seen, which demonstrates that our computational scenario can properly sample the tracer distribution during the combined LD–FD searches.

III. RESULTS

A. Dynamic behavior of full FD versus full LD search

In this section, we show first our results for the limiting full FD and full LD searches. The MFPT computed from the simulations is presented in Fig. 3(a). The circular and square open symbols depict τ_3 for the full FD MFPT and τ_1 for the full LD MFPT, respectively, both as a function of the inverse of the target size l_t^{-1} . The friction ratio here is set to $q = 1$, expecting in general that the LD search would be slower due to the confined geometry than the FD search in the free space (discussed also in Sec. II C). However, this applies only to the larger targets, while for the smaller targets we

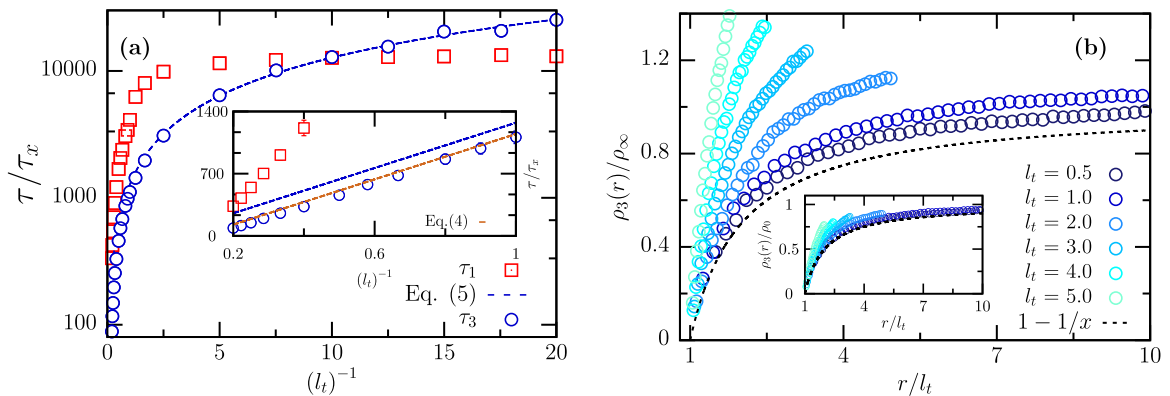


FIG. 3. (a) Simulation results for the target search time τ as a function of the inverse of the target size l_t^{-1} , normalized by τ_x . The y axis is plotted in log scale. All the results are for the friction ratio $q = 1$. The red squares and blue circles depict the results for τ_1 in the full LD and τ_3 in the full FD search, respectively. The blue dashed line denotes the Smoluchowski search time τ_{Smo} calculated from Eq. (5). In the inset, the search time τ_3 is shown in the range of $0.2 < 1/l_t < 1$. The theoretical prediction τ_{Smo} deviates from the simulation results, which is corrected (brown dashed line) by incorporating the finite system size $L = 10$ into Eq. (4). (b) The tracer concentration distribution function $\rho_3(r)$ in the full FD search, where r refers to the dimensionless tracer-target radial distance. The y and x axes are normalized by the tracer bulk concentration ρ_∞ and the target size l_t , respectively. The different colors depict the corresponding target size ranging from $l_t = 0.5$ to $l_t = 5.0$. The black dashed line denotes the concentration profile predicted by the Smoluchowski theory. In the inset, $\rho_3(r)$ is alternatively normalized by the rescaled bulk density $\rho_0 = \rho_\infty[L/(L - l_t)]$, which properly addresses the finite-size effect.

observe smaller τ_1 than τ_3 ; i.e., a set of 1D diffusion search is faster than continuous 3D search. This result indeed suggests that the target search time correlates not only with the type of diffusion, but also with the target size, as we will discuss further in the next section, particularly for τ_1 .

The theoretical prediction for τ_3 from the Smoluchowski law, Eq. (5), is shown by the dashed blue line in Fig. 3(a), in a good agreement with the simulation result depicted by the blue circles. In the regime of the large target size, $0.2 < 1/l_t < 1$, as shown in the inset, the simulation result underestimates the prediction. This discrepancy is due to the finite size of the system, and is fully resolved after inclusion of a correction term $1/L$ in Eq. (4), as shown by the brown dashed line in the inset of Fig. 3(a).

In addition, the tracer concentration distribution $\rho_3(r)$ for the full FD ($p_{\text{on}} = 0$ and $p_{\text{off}} = 1$) as a function of the tracer-target radial distance r is computed. The computed distribution ρ_3 is subject to boundary conditions of a constant tracer concentration $\rho_3(r = L) = \rho_0$ at the simulation box margin ($r = L$) and vanishing $\rho_3(r = l_t) = 0$ at the target surface ($r = l_t$). To this end, in the beginning of the simulation, we put N independent and pointlike tracer particles randomly at the box boundary ($r = L$). We then updated the simulation by adding a new tracer to the system analogously at the box boundary whenever an existing tracer adsorbs to the target. To ensure stationarity, we considered the production run simulation data only, in which the measured ρ_3 does not change with respect to the simulation time. According to the Smoluchowski theory, the stationary solution of ρ_3 should follow $\rho_3(r) = \rho_\infty(1 - l_t/r)$, given an infinitely large system, which defines a time-independent steady-state current pointing to the target. Here, $\rho_\infty = N/V$ refers to the reference number density of the tracer, corresponding to the bulk density of an infinitely large system. In Fig. 3(b), the normalized distribution $\rho_3(r)/\rho_\infty$ is plotted for the Smoluchowski theory (dashed line) and the simulation (circles), where the distance r on the x axis is rescaled by the target size l_t . The simulation results with small target sizes $l_t = 0.5$ and 1.0 accordingly exhibit the Smoluchowski tendency $y = 1 - 1/x$. However, finite size-effects emerge as l_t increases further, marked by a notable deviation between the simulation and the theory, in particular close to the lattice boundary for large targets with $l_t \geq 2$.

Now we want to formulate the tracer concentration distribution $\rho_3(r)$ applied to the finite-size system characterized by the lattice size L and the target size l_t . Recalling the related target search time τ_3 [Eq. (4)], one can incorporate the finite-size effect in terms of a rescaled bulk density $\rho_0 = \rho_\infty L/(L - l_t)$ and write the distribution function as $\rho_3 = \rho_0(1 - l_t/r)$ similarly to the Smoluchowski theory. In the inset of Fig. 3(b), the same simulation data are shown, now normalized by the rescaled density ρ_0 . The data for all different target sizes roughly collapse into a universal line $y = 1 - 1/x$, which validates our proposed concentration function $\rho_3(r)$ suitable for a finite-size system.

B. Dynamical features of the full LD search

As opposed to the full FD search, where τ_3 depends only linearly on l_t^{-1} , we have seen that the dynamic behavior of

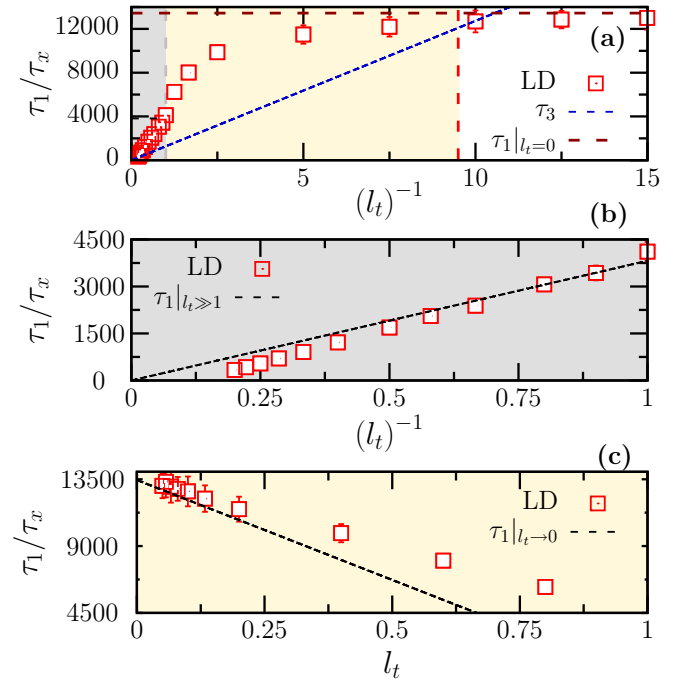


FIG. 4. (a) The MFPT of the full LD search τ_1 versus the inverse target size l_t^{-1} , normalized by τ_x , respectively. The red squares depict the simulation results. The horizontal brown line, the blue line, and the vertical red line denote the theoretical values of τ_3 [Eq. (4)], $\tau_1|_{l_t=0}$ [Eq. (6)], and l_{t2}^* via Eq. (13), respectively. The areas colored with light gray, yellow, and white highlight the regions of target size $1 < l_t, l_{t2}^* < l_t < 1$, and $l_t < l_{t2}^*$, respectively. The blue dashed line refers to the full FD search time τ_3 calculated by Eq. (4). Panels (b) and (c) depict the comparison of the simulation and theory in the range of $l_t > 1$ and in the range of $l_t < 1$, respectively. The black dashed lines correspond to the theoretical curve of $\tau_1|_{l_t \gg 1}$ via Eq. (7) in (b), and $\tau_1|_{l_t \rightarrow 0}$ via Eq. (10) in (c).

the LD search is more complicated. Figure 4(a) presents the simulation results for τ_1 versus the inverse target size l_t^{-1} in more detail. For small values of l_t^{-1} , as shown in Fig. 4(b), τ_1 increases with l_t^{-1} in a linear fashion, similarly to the full FD search. Yet, the increase becomes suppressed as l_t^{-1} further increases beyond $l_t^{-1} \approx 1$, and finally saturates as $l_t^{-1} \gtrsim 10$. This behavior of τ_1 is quite distinct from τ_3 , which diverges as l_t^{-1} increases.

As l_t decreases to zero, the target reduces to a lattice point with the corresponding search time expressed in Eq. (6). We depict $\tau_1|_{l_t=0}$ by the horizontal dashed brown line in Fig. 4(a), showing a good agreement with the simulation result, which asymptotically converges to the theoretical prediction. We also depict the full FD search time τ_3 by the blue dashed line in Fig. 4(a). A crossing point between $\tau_1|_{l_t=0}$ and τ_3 found around $l_t^{-1} \simeq 10$ indicates a characteristic target size defined by l_{t2}^* , under which τ_1 is smaller than τ_3 . After equalizing $\tau_3 = \tau_1|_{l_t=0}$, the corresponding target size is determined as

$$l_{t2}^* = \frac{q}{2\pi H(\mathbf{r}_S|\mathbf{r}_S)}. \quad (13)$$

For a cubic lattice with the periodic boundary conditions in all directions, one has $H(\mathbf{r}_S|\mathbf{r}_S) \simeq 1.516$ [42,59], leading to $1/l_{t2}^* = 9.53$ in the case of $q = 1$, which is close to our

findings. In fact, Eq. (13) is obtained by neglecting the finite-size term $1/L$ in Eq. (4) and the pseudo-Green's function $H(\mathbf{r}_S|\mathbf{r}_T)$ in Eq. (6); thus the finite-size effect is not considered. Nevertheless, l_{t2}^* still agrees very well with the simulation results, as we depict l_{t2}^* by the vertical red dashed line in Fig. 4(a).

Recalling Eqs. (7) and (10) which provide distinct expressions for the LD search time τ_1 as $l_t > 1$ and $l_t < 1$, the marginal length scale $l_{t1}^* \equiv 1$ is defined as it plays a decisive role in characterizing the dynamical behavior of the full LD search. In the range of $l_t > l_{t1}^*$, as also depicted by the gray area in Fig. 4(a), the target search time τ_1 is plotted versus the inverse target size l_t^{-1} in Fig. 4(b). Interestingly, the simulation result for τ_1 is found increasing almost linearly with respect to l_t^{-1} , similarly to the Smoluchowski theory for the full FD search. A quantitative agreement is revealed between the simulated τ_1 and the theoretical prediction Eq. (7) [dashed line in Fig. 4(b)], while the latter is derived for a sufficiently large target traced under random walks. Given the similar functional form for the full LD and full FD searches, a closer inspection is made of the respective slope $d(\tau_1/\tau_x)/d[(l_t)^{-1}]$. On the basis of the theoretical expression Eq. (7) and Eq. (4), using $q = 1$, one can find the slope $3N/(2\pi)$ and $N/(2\pi)$ for LD and FD, respectively. In other words, in the range of $l_t > l_{t1}^*$ and with the same friction coefficient, the LD search is three times slower than FD, but its dependency on the target size is similar to FD.

Now we focus on τ_1 for the target size below the critical target size, $l_t < l_{t1}^* = 1$. In Fig. 4(c), the simulation result for search time τ_1/τ_x is plotted as a function of the target size l_t . A linear dependence of τ_1 versus l_t is revealed, which is in sharp contrast to the above linear relation of τ_1 with l_t^{-1} separated by the marginal scale l_{t1}^* . In Eq. (10), we derive the asymptotic expression of τ_1 in the limit of $l_t \rightarrow 0$. Again, this solution is found in a good agreement with the simulation results, as depicted by the black dashed line in Fig. 4(c).

The critical length scale $l_{t1}^* = 1$ in the full LD signifies a subtle balance between the target radius and the network mesh size. Compared to the full FD search, where the entire surface area of the target is accessible for the tracer, the tracer in the full LD regime essentially searches for discrete target-chain intersection areas of total number N_{isec} [cf. Fig. 1(c)]. For $l_t > l_{t1}^*$, the expanding target leads to a roughly quadratic growth of N_{isec} in terms of the target size l_t , approaching a similar tendency than in the full FD search. However, for $l_t < l_{t1}^*$, the target surface is within the six nearest cross-links next to the center vertex of the lattice (see Fig. 1), which gives rise to the fixed number $N_{\text{isec}} = 6$. This is probably responsible for the distinct dynamic dependence on l_t between the search times $\tau_1|_{l_t \rightarrow 0}$ and $\tau_1|_{l_t \gg 1}$, which turns out to be a unique feature for the full LD search.

C. Dynamical features of the combined LD-FD searches

Finally, we focus on the case with the nonzero desorption probability p_{off} ; namely, the tracer is able to switch between the bound and unbound state with the lattice.

In Fig. 5, the simulated target search time τ with the fixed friction ratio $q = 1$ is shown as a function of the desorption probability p_{off} and of various target sizes. For the small

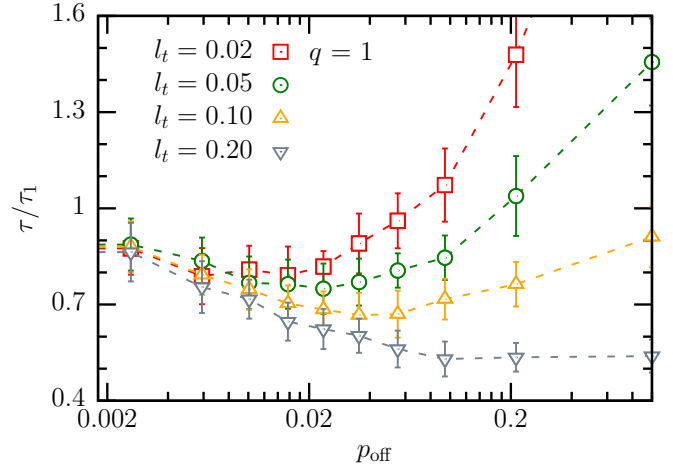


FIG. 5. Simulation results for the target search time τ versus the desorption probability p_{off} with a fixed friction ratio $q = 1$. τ is normalized with the full LD search time τ_1 with the desorption probability $p_{\text{off}} = 0$. The data points are computed from simulations with the rescaled target size ranging from $l_t = 0.02$ to 0.2 . The x axis is shown in log scale for better visualization.

target of the radius $l_t < 0.1$, the target search time exhibits a marked nonmonotonic nature in the range of $0 < p_{\text{off}} < 1$, implying the potential to optimize the search process after a proper mixing of the FD and LD searches. In the case of the target size $l_t = 0.02$, the minimum search time is achieved with the probability $p_{\text{off}}^* \simeq 0.02$. The resultant search time τ is found shorter by 28% and 72% of that for the full LD and the full FD searches, respectively. On the contrary, for larger target sizes above 0.1 , the search time τ is found to only monotonically decrease as p_{off} increases and converges to full FD search time. In the case of $l_t = 0.1$, the nonmonotonic behavior is not so strong, implying that a marginal target size around $l_m \equiv 0.1$ plays the role of a characteristic length that determines whether the combined LD-FD search becomes favorable or not.

Apparently, the above marginal target size $l_m = 0.1$ is not a universal value but depends on other system parameters. We already know that the critical target size l_{t2}^* plays an analogous role to l_m in assessing the relative efficiency of the FD and LD search. Specific to the above case, $l_{t2}^* = 0.105$ is found with the same value as l_m . Thus, we propose a genetic relation $l_m = l_{t2}^*$, which further follows the critical friction ratio q^* :

$$q^* = 2\pi H(\mathbf{r}_S|\mathbf{r}_S)l_t. \quad (14)$$

In analogy to l_m , q^* serves as an indicator to the efficiency of the combined LD-FD search. Given the relation $H(\mathbf{r}_S|\mathbf{r}_S) \simeq 1.516$ for the cubic lattice and the target radius $l_t = 0.02$, the combined LD-FD search becomes feasible under the condition $q > q^* = 0.0145$. The above discussion is relevant also for cases of a biomolecule sliding on 1D chains, for instance, protein sliding on the DNA, where the related friction coefficient for LD is known to be orders of magnitude larger than those for the FD [1]. The related friction ratio q is surprisingly in a similar order of magnitude to the q^* derived for the cubic lattice.

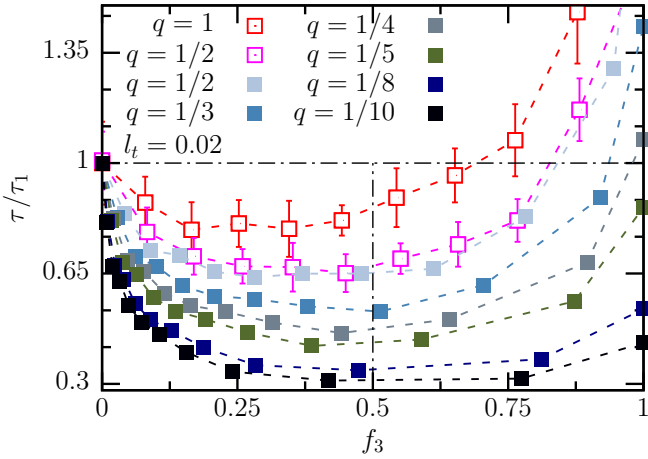


FIG. 6. Simulation results for the target search time τ as a function of the FD search time fraction f_3 for the combined LD-FD search. τ is normalized with the full LD search time τ_1 . The open symbols correspond to the simulation results with the friction ratios $q = 1$ and $q = 1/2$, respectively. The results for even smaller q are obtained via the FD search time rescaling from $\tau|_{q=1}$, according to Eq. (15) (see the text for details), as displayed with filled symbols until $q = 1/10$ in the plot. The target size is fixed to $l_t = 0.02$ here.

We should stress that although the adjustment of the target size and the friction ratio both result in a nonmonotonic dependence of the search time with p_{off} , they signify completely different processes. The target radius l_t determines the accessible area to the tracer and thus alters the search process. Yet, tuning the friction ratio q essentially alters the dynamic performance of the LD and FD searches. In the case of our model, where we fix the LD friction coefficient γ_1 and leave γ_3 free, varying the friction ratio from $q = 1$ to q' essentially rescales the average FD search time included in one search course from $\omega_3|_{q=1}$ to $q'\omega_3|_{q=1}$, while the LD search time remains intact. And importantly, the resultant desorption probability should effectively change to $q'p_{\text{off}}|_{q=1}$ due to the time step change. The summation of the FD and LD search time yields the overall search time $\tau|_{q'} = \omega_1|_{q=1} + q'\omega_3|_{q=1}$, and equivalently,

$$\tau|_{q'} = \tau|_{q=1}\{f_3|_{q=1} \cdot q' + (1 - f_3|_{q=1})\}, \quad (15)$$

which is expressed as a function of the time fraction f_3 for the FD search previously defined in Eq. (12).

In Fig. 6, we present the simulation results for the target search time τ as a function of the fraction f_3 , after normalized by τ_1 of the full LD search. The target size is fixed to $l_t = 0.02$. The red open squares depict the simulation results of τ with $q = 1$, clearly showing the nonmonotonicity where the optimal time fraction is $f_3^* \simeq 0.3$. The pink open squares depict the simulation result τ with $q = 1/2$, whereas the gray solid squares refer to $\tau|_{q'=1/2}$ after a time rescaling from $\tau|_{q=1}$ as shown in Eq. (15). The revealed good agreement at $q = 1/2$ validates the derived rescaling scheme. We further generate the search time below $q = 1/2$, as depicted by the filled squares in Fig. 6. The nonmonotonicity of τ becomes profound for intermediate q , indicating the possible optimization of the LD-FD search. To compare the LD-FD search with the full LD and full FD searches, we

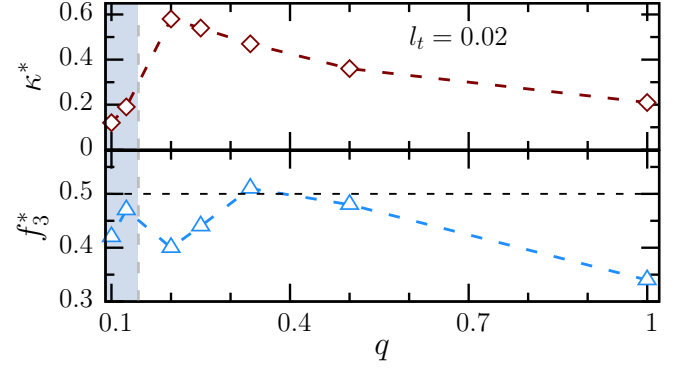


FIG. 7. Upper panel: The time reduction ratio κ^* as a function of the friction ratio q . Lower panel: The time occupation ratio f_3^* for the FD search extracted from the search time minimum exhibited in Fig. 6, as a function of the friction ratio q . The area colored in blue (for very low q) highlights the regime of $q < q^*$, where the critical ratio q^* is calculated via Eq. (14).

first determine the optimal search time $\tau_{\text{mono}} = \text{Min}\{\tau_1, \tau_3\}$ via a single search mode, then $\kappa^* = 1 - \tau^*/\tau_{\text{mono}}$ reads the fraction of the time reduced by the combined LD-FD approach, where τ^* is the minimal search time τ revealed as a function of the probability p_{off} . Consequently, κ^* is read off as $\kappa^* \simeq 35\%$ with $q = 1/2$, which increases to $\kappa^* \simeq 50\%$ with $q = 1/3$.

The time reduction ratio κ^* and the corresponding time fraction f_3^* for $l_t = 0.02$ are presented as a function of q in Fig. 7. It appears that κ^* , which signifies the efficiency of the combined LD-FD search, first increases with decreasing q from 1 but then drops down below $q \simeq 0.24$. At the transition point $q \simeq 0.24$, the combined LD-FD search becomes the most efficient with $\kappa^* \simeq 58\%$, implying that the combined LD-FD search can save at most more than half of the search time than that from a single search mode. The vertical dashed line depicts the critical q^* derived from Eq. (14), which nicely agrees with the simulation results suggesting the efficiency of the combined LD-FD search should decrease as $q < q^*$. Interestingly, the ratio f_3^* is found close to 0.5 as $q^* < q < 0.55$, suggesting that the target search process is optimized at the point where involved LD and FD search times become comparable.

IV. DISCUSSION

By means of theory and numerical simulations, we have studied the target search process of a diffusing pointlike tracer in a 3D lattice, modeling a polymer network. To illustrate the underlying physics, our findings are now discussed in a more qualitative manner. First, we should recall the fact that the 1D diffusion is recurrent, which may repeatedly visit the same point, whereas the 3D diffusion is not. Therefore, the 3D diffusion could be more suitable for a long-range search. On the other hand, the trapping of the tracer to the chain lattice decreases the search space for the LD search. Therefore, the 1D diffusion could be more beneficial for a detailed local search. The interplay of these two effects motivates applications of the combined 1D-3D search, which turned out to be optimal in many circumstances, for instance, in surface-mediated diffu-

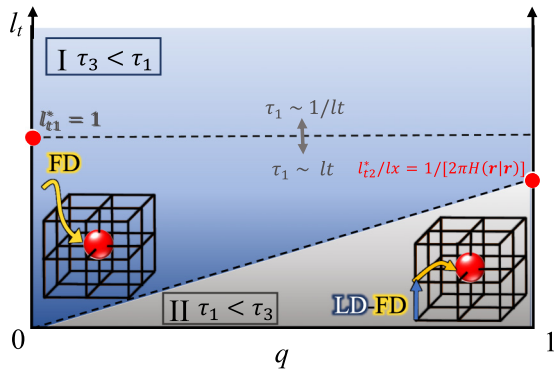


FIG. 8. Diagram of regimes indicating the favorable search strategy. The x and y axes denote the fraction coefficient ratio q ranging from 0 to 1 and the target radius l_t , respectively. The FD search is optimal in regime I, whereas in regime II the combined LD-FD search becomes favorable driven by the optimal tracer desorption probability p_{off} . The boundary of these two regimes is depicted by the black dashed oblique line according to Eq. (13). The horizontal dashed line depicts the critical target size $l_{t1}^* = 1$ for the LD search, crossing which the expression of full LD search time τ_1 holds a different scaling law with the target size.

sion [60–62]. Our work extends previous studies on pointlike targets by introducing a target of adjustable size placed on the lattice cross-linker. In the limit of a pointlike target, i.e., $l_t = 0$, the LD search reduces to a random search process on a pure cross-linked lattice, enabling us to analytically solve the target search time that is finite in contrast with the diverging search time for the FD search. Therefore, it is plausible to expect that the LD search is more efficient in certain small length scales of l_t than the FD search, particularly for targets with the finite size $0 < l_t < 1$ where the target remains 6 intersection points with the lattice. For the larger target size $l_t > 1$, where the number of chain-target intersection points increase with the expanding target, one can infer that the LD search behaves similarly to the FD, as confirmed by our results.

The quantitative assessment of the target search time relies on the friction coefficient and thus the diffusion coefficient of the tracer. We formulate the search time as a function of the friction coefficient and the target size between the FD and the LD search. We obtained a critical target size signifying the length scale below which the LD search becomes more favorable, which is exemplified by the simulations as well. In this study, we focus on systems with a large friction in the LD and a small friction in the FD. Thus, the LD search is likely to be optimized under certain conditions with the combination of the FD search. We found that the combined LD-FD search becomes optimal in the regime characterized via an upper bound of the target size l_{t2}^* and a lower bound of the friction coefficient ratio q . That is highlighted thorough the triangular regime in the (q, l_t) phase space as indicated in Fig. 8. The red point on the right denotes the critical target size $l_{t2}^* = 1/[2\pi H(r|r)]$ at the ratio $q = 1$, derived from Eq. (13). We attribute this optimization mechanism to the situation where the fast FD search may quickly deliver the tracer close to the target before performing the slow but detailed LD search

that turns out to be more efficient for small targets. We have found that a maximum of 50% of the search time can be saved by the combined LD-FD search relative to the case with full LD or full FD search. However, the reduction factor reported in experiments is usually based on the FD search limit [1], which can be very large with very small targets. Moreover, the coiled and flexible nature of DNA networks plays a critical role for the feasibility of the combined LD-FD search [19], making the intermittent search possibly more efficient in the network of flexible chains or in an imperfect lattice with defects.

Note also that here our chain network based on the cubic lattice is a model on the simplest level. The flexibility of the chain, the chemical components of the polymer, as well as the heterogeneity of the polymer structure are all ignored in the current work, which may further add important corrections to the target search time. However, this minimal polymer network model captures most salient features of complex gels, as similarly and previously considered [44,45]. As a result, the measure of the target search time remains on a level affordable for computational studies. Apart from that, our model focuses on the target fixed at the cross-link in the center of the box. This facilitates the development of theoretical tools, for instance the random walk theory in the lattice, but does not necessarily represent general occasions where the target could be placed elsewhere. A good example for that is to compare the target placed in the middle of the chain and on the cross-link, where the relevant LD search time has already been very different in the limit of $l_t \rightarrow 0$. Nevertheless, the dynamic features uncovered here of the FD, LD, and combined LD-FD search should apply to targets with a generic placement.

V. CONCLUSIONS

To conclude, we have studied the target search process of a diffusing pointlike tracer in a 3D spatial lattice modeling polymer networks. The target is fixed at one lattice cross-link in the center of the simulation box, and the tracer can conditionally associate and dissociate with the polymer chain along the tracing pathway. Our study quantifies the dependence of the target search time on the target size and the friction coefficient of the tracer. Critical target sizes are revealed regulating the efficiency of the LD, the FD, and the combined LD-FD search. In particular, we have found under certain conditions that the search can be optimized via the combined LD-FD search, which saves up to 50% of the search time relative to the cases of full LD or full FD search.

As one may notice, the combined LD-FD search in our study is in spirit similar to the sliding-hopping dynamics observed in many biological systems. The relation $k_{\text{off}} = p_{\text{off}}^* \gamma_1 / \gamma_1^{\text{exp}}$ can provide a rough translation of the optimal desorption probability p_{off}^* into the desorption rate k_{off} for the tracer [19]. Further applications, for instance, to nanoreactors where small catalytic targets are immobilized in the polymer network [28] and the metal-organic frameworks (MOFs) [29,36], should be relevant to this study. In particular, the underlying theoretical predictions discussed in this work could be useful for designing the catalyst and polymer network

conjugate structures, aiming at the optimization of a desired catalytic activity.

ACKNOWLEDGMENTS

The authors thank Yonghyun Song and Stefano Angioletti-Uberti for fruitful discussions. The authors also thank the referees for the very constructive feedback which helped significantly to improve the contents and presentation of our work. This project has received funding from the European Research Council (ERC) under the European Union's Horizon 2020 research and innovation program (Grant Agreement No. 646659). X.X. thanks the National Science Foundation of China (Grant No. 21903045), China Postdoctoral Science Foundation (Grant No. 2019M661842), and the Fundamental Research Funds for the Central Universities (Grant No. 30920021122) for financial support. W.K.K. acknowledges the support by KIAS Individual Grant No. CG076001 at Korea Institute for Advanced Study.

APPENDIX: PSEUDO GREEN'S FUNCTION

We consider the Laplacian operator [42]

$$(-\Delta)_{ij} = \delta_{ij} - w_{ij}, \quad (\text{A1})$$

$$H(\mathbf{r}|\mathbf{r}') = \frac{1}{N} \sum_{m=0}^{N_L-1} \sum_{n=0}^{N_L-1} \sum_{p=\delta(m,n)(0,0)}^{N_L-1} \times \frac{\exp[2im\pi(x-x')/N_L + 2in\pi(y-y')/N_L + 2ip\pi(z-z')/N_L]}{1 - \frac{1}{3}[\cos(2m\pi/N_L) + \cos(2n\pi/\tilde{L}) + \cos(2p\pi/\tilde{L})]}. \quad (\text{A3})$$

Here, the cubic lattice consists of $N_L = 2\tilde{L} + 1$ lattice points in each direction. The target and the initial position of the tracer are labeled with the position vector \mathbf{r} and \mathbf{r}' , with the integral coordinates (x, y, z) and (x', y', z') , respectively. The imaginary part in the exponential term of Eq. (A3) will self-cancel over the summation on m, n, p .

where δ_{ij} is the Kronecker symbol and w_{ij} refers to the symmetric transition rate of the tracer from lattice point i to j . The operator Δ_{ij} applies to N cross-links at the finite-size lattice subject to the periodic cubic box in all directions. The pseudo-Green's function on the lattice is then defined as [63]

$$(-\Delta)_{ij}H(\mathbf{r}_i|\mathbf{r}_j) = \delta(\mathbf{r}_i - \mathbf{r}_j) - \phi^{(0)*}(\mathbf{r}_i) \times \phi^{(0)}(\mathbf{r}_j). \quad (\text{A2})$$

Note that $\phi^i(\mathbf{r})$ defines the i th eigenfunction of the operator $(-\Delta)_{ij}$ with the eigenvalue λ_i . Index i ranges for N possible eigenfunctions from 0 to $N - 1$. The pseudo-Gaussian function $H(\mathbf{r}_i|\mathbf{r}_j)$ differs from the conventional Gaussian function via the product $(-\phi^{(0)*} \times \phi^{(0)})$, corresponding to the underlying lattice with finite size and periodic boundaries [42,63].

Particularly for the 3D simple cubic lattice under study, the analytical expression of $H(\mathbf{r}|\mathbf{r}')$ can be obtained via the Fourier analysis via the equation [42]

-
- [1] A. B. Kolomeisky, *Phys. Chem. Chem. Phys.* **13**, 2088 (2011).
 - [2] C. A. Kaiser, M. Krieger, H. Lodish, and A. Berk, *Molecular Cell Biology* (W. H. Freeman, New York, 2007).
 - [3] C. Loverdo, O. Bénichou, M. Moreau, and R. Voituriez, *Nat. Phys.* **4**, 134 (2008).
 - [4] O. Bénichou, C. Loverdo, M. Moreau, and R. Voituriez, *Rev. Mod. Phys.* **83**, 81 (2011).
 - [5] G. M. Viswanathan, S. V. Buldyrev, S. Havlin, M. Da Luz, E. Raposo, and H. E. Stanley, *Nature (London)* **401**, 911 (1999).
 - [6] A. M. Edwards, R. A. Phillips, N. W. Watkins, M. P. Freeman, E. J. Murphy, V. Afanasyev, S. V. Buldyrev, M. G. da Luz, E. P. Raposo, H. E. Stanley *et al.*, *Nature (London)* **449**, 1044 (2007).
 - [7] M. F. Shlesinger, *J. Phys. A: Math. Theor.* **42**, 434001 (2009).
 - [8] F. Bartumeus, *Oikos* **118**, 488 (2009).
 - [9] M. A. D. de la Rosa, E. F. Koslover, P. J. Mulligan, and A. J. Spakowitz, *Biophys. J.* **98**, 2943 (2010).
 - [10] F. Höfling and T. Franosch, *Rep. Prog. Phys.* **76**, 046602 (2013).
 - [11] P. H. Richter and M. Eigen, *Biophys. Chem.* **2**, 255 (1974).
 - [12] O. G. Berg and C. Blomberg, *Biophys. Chem.* **4**, 367 (1976).
 - [13] A. D. Riggs, S. Bourgeois, and M. Cohn, *J. Mol. Biol.* **53**, 401 (1970).
 - [14] M. Smoluchowski, *Phys. Z.* **17**, 557 (1916).
 - [15] M. A. Lomholt, K. Tal, R. Metzler, and K. Joseph, *Proc. Natl. Acad. Sci. USA* **105**, 11055 (2008).
 - [16] O. Bénichou, C. Loverdo, M. Moreau, and R. Voituriez, *Phys. Rev. E* **74**, 020102(R) (2006).
 - [17] O. G. Berg, R. B. Winter, and P. H. Von Hippel, *Biochemistry* **20**, 6929 (1981).
 - [18] U. Gerland, J. D. Moroz, and T. Hwa, *Proc. Natl. Acad. Sci. USA* **99**, 12015 (2002).
 - [19] S. E. Halford and J. F. Marko, *Nucl. Aci. Res.* **32**, 3040 (2004).
 - [20] A. Tafvizi, L. A. Mirny, and A. M. van Oijen, *ChemPhysChem* **12**, 1481 (2011).
 - [21] T. Hu, A. Y. Grosberg, and B. Shklovskii, *Biophys. J.* **90**, 2731 (2006).
 - [22] J. Smrek and A. Y. Grosberg, *Phys. Rev. E* **92**, 012702 (2015).
 - [23] M. Slutsky and L. A. Mirny, *Biophys. J.* **87**, 4021 (2004).
 - [24] L. Mirny, M. Slutsky, Z. Wunderlich, A. Tafvizi, J. Leith, and A. Kosmrlj, *J. Phys. A: Math. Theor.* **42**, 434013 (2009).
 - [25] J. Hansing and R. R. Netz, *Macromolecules* **51**, 7608 (2018).
 - [26] Y. Lu, Y. Mei, M. Drechsler, and M. Ballauff, *Angew. Chem. Int. Ed.* **45**, 813 (2006).
 - [27] Y. Lu and M. Ballauff, *Prog. Polym. Sci.* **36**, 767 (2011).
 - [28] P. Herves, M. Pérez-Lorenzo, L. M. Liz-Marzán, J. Dzubiella, Y. Lu, and M. Ballauff, *Chem. Soc. Rev.* **41**, 5577 (2012).
 - [29] D. Wu, F. Xu, B. Sun, R. Fu, H. He, and K. Matyjaszewski, *Chem. Rev.* **112**, 3959 (2012).

- [30] G. Prieto, H. Tüysüz, N. Duyckaerts, J. Knossalla, G.-H. Wang, and F. Schüth, *Chem. Rev.* **116**, 14056 (2016).
- [31] J.-T. Zhang, G. Wei, T. F. Keller, H. Gallagher, C. Stötzl, F. A. Müller, M. Gottschaldt, U. S. Schubert, and K. D. Jandt, *Macromol. Mater. Eng.* **295**, 1049 (2010).
- [32] R. Contreras-Cáceres, A. Sánchez-Iglesias, M. Karg, I. Pastoriza-Santos, J. Pérez-Juste, J. Pacifico, T. Hellweg, A. Fernández-Barbero, and L. M. Liz-Marzán, *Adv. Mater.* **20**, 1666 (2008).
- [33] S. Carregal-Romero, N. J. Buurma, J. Pérez-Juste, L. M. Liz-Marzán, and P. Hervés, *Chem. Mater.* **22**, 3051 (2010).
- [34] H. Jia, R. Roa, S. Angioletti-Uberti, K. Henzler, A. Ott, X. Lin, J. Möser, Z. Kochovski, A. Schnegg, J. Dzubiella, M. Ballauff, and Y. Lu, *J. Mater. Chem. A* **4**, 9677 (2016).
- [35] S. Li, D. Lin, J. Zhou, and L. Zha, *J. Phys. Chem. C* **120**, 4902 (2016).
- [36] S. Kitagawa, R. Kitaura, and S.-I. Noro, *Angew. Chem. Int. Ed.* **43**, 2334 (2004).
- [37] R. Roa, S. Angioletti-Uberti, Y. Lu, J. Dzubiella, F. Piazza, and M. Ballauff, *Z. Phys. Chem.* **232**, 773 (2018).
- [38] R. Roa, W. K. Kim, M. Kanduč, J. Dzubiella, and S. Angioletti-Uberti, *ACS Catal.* **7**, 5604 (2017).
- [39] M. Galanti, D. Fanelli, S. Angioletti-Uberti, M. Ballauff, J. Dzubiella, and F. Piazza, *Phys. Chem. Chem. Phys.* **18**, 20758 (2016).
- [40] J. D. Noh and H. Rieger, *Phys. Rev. Lett.* **92**, 118701 (2004).
- [41] S. Condamin, O. Bénichou, and M. Moreau, *Phys. Rev. Lett.* **95**, 260601 (2005).
- [42] S. Condamin, O. Bénichou, and M. Moreau, *Phys. Rev. E* **75**, 021111 (2007).
- [43] S. Condamin and O. Bénichou, *J. Chem. Phys.* **124**, 206103 (2006).
- [44] J. Hansing, C. Ciemer, W. K. Kim, X. Zhang, J. E. DeRouchey, and R. R. Netz, *Eur. Phys. J. E* **39**, 53 (2016).
- [45] X. Zhang, J. Hansing, R. R. Netz, and J. E. DeRouchey, *Biophys. J.* **108**, 530 (2015).
- [46] P. H. von Hippel, *Annu. Rev. Biophys. Biomol. Struct.* **36**, 79 (2007).
- [47] V. Dahirel, F. Paillusson, M. Jardat, M. Barbi, and J.-M. Victor, *Phys. Rev. Lett.* **102**, 228101 (2009).
- [48] C. Fröhner and F. Noé, *J. Phys. Chem. B* **122**, 11240 (2018).
- [49] J. Tringe, N. Ileri, H. Levie, P. Stroeve, V. Ustach, R. Faller, and P. Renaud, *Chem. Phys.* **457**, 19 (2015).
- [50] D. Krepel, D. Gomez, S. Klumpp, and Y. Levy, *J. Phys. Chem. B* **120**, 11113 (2016).
- [51] J. Shin and A. B. Kolomeisky, *J. Chem. Phys.* **151**, 125101 (2019).
- [52] S. Jabbari-Farouji and E. Trizac, *J. Chem. Phys.* **137**, 054107 (2012).
- [53] T. Ooppelstrup, V. V. Bulatov, A. Donev, M. H. Kalos, G. H. Gilmer, and B. Sadigh, *Phys. Rev. E* **80**, 066701 (2009).
- [54] M. Doi and S. F. Edwards, *The Theory of Polymer Dynamics* (Oxford University Press, Oxford, 1988).
- [55] P. Hammar, P. Leroy, A. Mahmutovic, E. G. Marklund, O. G. Berg, and J. Elf, *Science* **336**, 1595 (2012).
- [56] B. Bagchi, P. C. Blainey, and X. S. Xie, *J. Phys. Chem. B* **112**, 6282 (2008).
- [57] J. Elf, G.-W. Li, and X. S. Xie, *Science* **316**, 1191 (2007).
- [58] A. Szabo, K. Schulten, and Z. Schulten, *J. Chem. Phys.* **72**, 4350 (1980).
- [59] B. D. Hughes *et al.*, *Random Walks and Random Environments: Random Walks*, Vol. 1 (Oxford University Press, Oxford, 1995).
- [60] O. Bénichou, D. Grebenkov, P. Levitz, C. Loverdo, and R. Voituriez, *Phys. Rev. Lett.* **105**, 150606 (2010).
- [61] O. Bénichou, D. Grebenkov, P. Levitz, C. Loverdo, and R. Voituriez, *J. Stat. Phys.* **142**, 657 (2011).
- [62] G. Oshanin, M. Tamm, and O. Vasilyev, *J. Chem. Phys.* **132**, 235101 (2010).
- [63] G. Barton and G. Barton, *Elements of Green's Functions and Propagation: Potentials, Diffusion, and Waves* (Oxford University Press, Oxford, 1989).